Princeton Plasma Physics Laboratory

PPPL- 4833

PPPL- 4833

# Dependence of H-mode Energy Confinement and Transport on Collisionality in NSTX

S.M. Kaye, S. Gerhardt, W. Guttenfelder, R. Maingi, R.E. Bell, A. Diallo,
B.P. LeBlanc and M. Podesta

November, 2012

Prepared for the U.S. Department of Energy under Contract DE-AC02-09CH11466.

# Princeton Plasma Physics Laboratory
# Report Disclaimers

---

## Full Legal Disclaimer



## Trademark Disclaimer



---

# PPPL Report Availability

## Princeton Plasma Physics Laboratory:

http://www.pppl.gov/techreports.cfm

## Office of Scientific and Technical Information (OSTI):

http://www.osti.gov/bridge

---

**Related Links:**

**U.S. Department of Energy**

**Office of Scientific and Technical Information**

**Fusion Links**

# The Dependence of H-mode Energy Confinement and Transport on Collisionality in NSTX

S.M. Kaye[1], S. Gerhardt[1], W. Guttenfelder[1], R. Maingi[2], R.E. Bell[1], A. Diallo[1], B.P. LeBlanc[1], M. Podesta[1]

e-mail contact: kaye@pppl.gov

## Abstract

Understanding the dependence of confinement on collisionality in tokamaks is important for the design of next-step devices, which will operate at collisionalities at least one order of magnitude lower than in present generation. A wide range of collisionality has been obtained in the National Spherical Torus Experiment (NSTX) by employing two different wall conditioning techniques, one with boronization and between-shot helium glow discharge conditioning (HeGDC+B), and one using lithium evaporation (Li EVAP). Previous studies of HeGDC+B plasmas indicated a strong and favorable dependence of normalized confinement on collisionality. Discharges with lithium conditioning discussed in the present study generally achieved lower collisionality, extending the accessible range of collisionality by almost an order of unity. While the confinement dependences on dimensional, engineering variables of the HeGDC+B and Li EVAP datasets differed, collisionality was found to unify the trends, with the lower collisionality lithium conditioned discharges extending the trend of increasing normalized confinement time with decreasing collisionality when other dimensionless variables were held as fixed as possible. This increase of confinement with decreasing collisionality was driven by a large reduction in electron transport in the outer region of the plasma. This result is consistent with gyrokinetic calculations that show microtearing and Electron Temperature Gradient modes to be more stable for the lower collisionality discharges. Ion transport, near neoclassical at high collisionality, became more anomalous at lower collisionality, possibly due to the growth of hybrid TEM/KBM modes in the outer regions of the plasma.

---

[1]Princeton Plasma Physics Laboratory, Princeton University, Princeton, NJ 08543, USA
[2]Oak Ridge National Laboratory, Oak Ridge, TN 37831 USA

# I. Introduction

Parametric dependences of plasma confinement and transport can be based on sets of dimensional parameters that can be controlled experimentally,[1–3] or on dimensionless or "physics" variables that are believed to represent more accurately the underlying physics mechanisms controlling transport.[4,5] Examples of the former are plasma current, $I_p$, toroidal magnetic field, $B_T$, plasma density, $n_e$, and heating power, $P_{heat}$. At conventional aspect ratio (R/a$\sim$2.5 to 4.0), these dependences are captured by the ITER98y,2 confinement scaling,[6] with

$$\tau_{E,th} \sim I_p{}^{0.93} B_T{}^{0.15} \langle n_e \rangle^{0.41} P_{heat}^{-0.69} M^{0.19} R^{1.97} (a/R)^{0.58} \kappa^{0.78} \quad (1)$$

where $\tau_{E,th}$ is the thermal energy confinement time, $\langle n_e \rangle$ is volume-averaged electron density, $M$ is the main ion mass, $R$ is major radius, $a$ is minor radius and $\kappa$ is plasma elongation. The ITER98y,2 scaling has a strong plasma current but weak toroidal field dependence. In low aspect ratio devices such as NSTX or MAST, where $R/a \simeq 1.3$ to 1.4, the dimensional scalings showed reversed trends; for NSTX discharges that used Helium Glow Discharge Cleaning plus occasional boronization for wall conditioning (HeGDC+B), $\tau_{E,th} \sim I_p{}^{0.4} B_T{}^{1.01}$.[1–3]

The set of physics variables includes the normalized gyroradius, $\rho^*$ ($=\rho/a$) where $\rho$ is gyroradius , the plasma beta $\beta \sim p/B_T^2$, where $p$ is plasma pressure, and the normalized electron collisionality, $\nu_e^* \sim n_e Z_{eff}/T_e^2$ for fixed q and geometry. The collisionality reflects the physics of both resistive and trapped particle effects, while $\langle \beta_T \rangle$ could reflect the importance of electromagnetic effects. A recent review of the dependence of confinement on various dimensionless parameters[5] has, in fact, shown that by combining data from a range of devices, the collisionality dependence of normalized confinement, $B_T \tau_{E,th}$ is itself a function of collisionality, with weaker dependences at lower $\nu_e^*$.

The National Spherical Torus Experiment (NSTX) is a high-power, low aspect ratio tokamak. A large range of collisionality has been achieved in NSTX using various methods of wall conditioning. Early experiments were carried out with wall conditioning consisting of boronization and between-shot Helium Glow Discharge cleaning (HeGDC+B). More recently, NSTX has employed between-shots lithium conditioning of the vessel walls through evaporation from two LITERs (LIThium EvapoRators) mounted at the top of the NSTX vessel (Li EVAP).[7] It is important to note that the evaporated lithium generally remained outside the main plasma, and it did not contribute to the impurity content of the plasma.[8] The main impurity species for discharges using either wall conditioning technique was carbon.

Lithium conditioning, however, led to both lower collisionalities and to improvements in

energy confinement time during the H-mode, most notably in the electron channel.[9,10] It was found that the HeGDC+B and Li EVAP discharges scale differently with engineering parameters, but that these differing dependences can be reconciled by an underlying collisionality variation, which unifies both sets of data and which exhibits a strong improvement of normalized energy confinement with decreasing $\nu_e^*$. It is the purpose of this work to characterize and understand the causes of this collisionality dependence. This underlying dependence could potentially influence strongly the design and construction of an ST-based Fusion Nuclear Science Facility (FNSF),[11,12] as this class device will operate at collisionalities at least one order of magnitude lower than the operating range of NSTX in this parameter.

In the following sections we will present results of the global scaling of the confinement with collisionality. Then, we will discuss the underlying reasons for this trend, first by presenting changes in profiles and inferred transport, and then by putting these changes into the framework of the results of linear gyrokinetic-based microstability analysis.

## II. Datasets and Global Confinement Dependences

The discharges used for this study are all H-modes based on $I_p$, $B_T$ scans in plasmas using either HeGDC+B or Li EVAP wall conditioning, and a lithium deposition scan at fixed $I_p$ and $B_T$. The HeGDC+B discharges covered the range of $I_p$ from 0.7 to 1.1 $MA$, $B_T$ from 0.35 to 0.55 $T$, had deuterium neutral beam (NB) heating powers of $\sim 4$ $MW$ into Lower Single Null (LSN) deuterium plasmas, elongation, $\kappa$, $\sim 2.2$ and plasma densities up to $6 \times 10^{19}$ $m^{-3}$. All of these discharges exhibited small, Type V ELMs, which did not affect confinement significantly. An example of this type of discharge is shown in Fig. 1a. The L-H transition in this 4 $MW$ discharge occurred near t=210 ms, and the Type V ELMs started at 0.4 ms. Although the density continued to rise during the course of this discharge, the stored energy reached and maintained a level of approximately 200 kJoules, and the fraction of radiated to heating power, $P_{rad}/P_{heat}$ remained under 10% during the period of steady stored energy. Here, $P_{heat}$ is taken to be $P_{heat} = P_{OH} + P_{be} + P_{bi} - dW/dt$, where $P_{OH}$ is the ohmic heating power, $P_{be}$ and $P_{bi}$ are the beam collisional heating of the electrons and ions respectively, and $dW/dt$ is the time rate of change of the total stored energy in the plasma. Note that beam losses due to orbit effects, charge-exchange, shine-thru and slowing down are accounted for in this definition.

In Fig. 1b is shown the discharge evolution for a plasma in which Li evaporation was used for wall conditioning. The L-H transition occurred near 250 ms, and while the $D_\alpha$ signal remained high, no ELMs were observed in this particular discharge. In general, the Li EVAP discharges had longer pulse durations than did the HeGDC+B discharges. The

stored energy in this Li EVAP discharge remained nearly constant and was also 200 kJ, while the density in this discharge also was seen to rise continuously. Note here that the radiated power fraction increased to values near 40% by the end of the discharge. This increase in $P_{rad}/P_{heat}$, as well as the increasing $n_e$, was due primarily to carbon accumulation in the plasma core. The deuterium inventory for the Li EVAP discharges tended to remain constant during the current flattop.

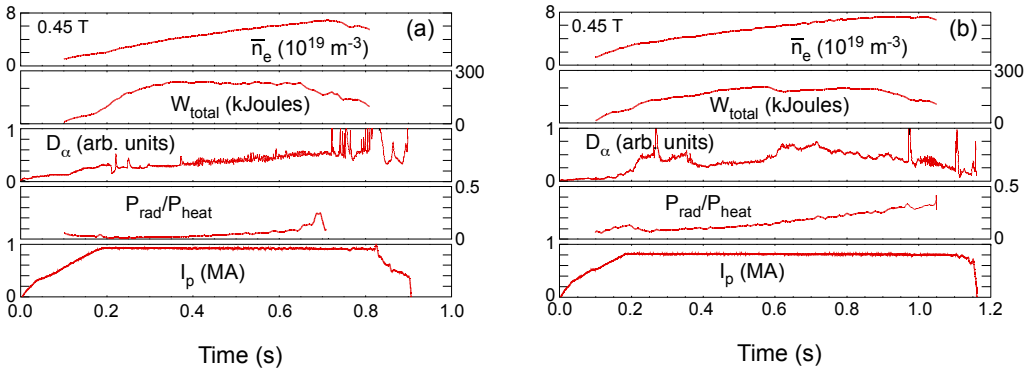


Figure 1: Discharge evolution for a plasma with a) HeGDC+B and b) Li evaporation wall conditioning. Shown from the top panel down are line-averaged electron density, total stored energy, $D_\alpha$ emission, fraction of radiated to heating power, and plasma current.

The Li EVAP discharges used in this study were obtained from results of several different experiments, all in the LSN configuration.[13,14] $I_p$ and $B_T$ scans were performed in sets of

discharges for which the between-shots lithium evaporation was held to between 90 and 270 mg. These discharges covered the range $I_p$=0.7 to 1.3 $MA$, $B_T$=0.34 to 0.54 $T$, $\kappa \sim 2.3$, and had NB heating powers of approximately 3 $MW$. The collection of discharges, with either HeGDC+B or Li EVAP wall conditioning in which $I_p$ and $B_T$ were varied is dubbed the "Nu scan". Another set of discharges was taken from a dedicated lithium evaporation scan (dubbed the "Li scan"), covering the range from 0 to 1000 $mg$ of lithium evaporated between shots at fixed $I_p = 0.8$ $MA$, $B_T = 0.44$ $T$ and $\kappa = 1.8$. The NB heating power in this latter set varied from 2.2 to 4.2 $MW$. While there were repetitive Type I ELMs at low levels of lithium, the ELMs disappeared at higher levels.[15] Confinement and transport levels for the analysis presented here were taken during inter-ELM periods (for lower deposition values), and thus the direct effect of ELMs was removed. Also, analysis times were taken during periods of steady stored energy and for $P_{rad}/P_{heat}$<20%.

As stated in the Introduction, the HeGDC+B and Li EVAP discharges exhibit engineering parameter dependences of confinement in H-mode plasmas that are different. This is shown in Fig. 2. The HeGDC+B plasmas (top row) show a strong, nearly linear dependence on $B_T$ with a weaker dependence on $I_p$, going as $I_p^{0.4} B_T^{0.9}$.[1–3] When transformed to dimensionless physics variables, the NSTX confinement scaling showed a strong increase, almost inverse linearly, with decreasing collisionality.[3] The dependences on both the engineering and physics parameters observed in NSTX were also observed on the MAST spherical tokamak.[16,17] The Li EVAP discharges on NSTX (bottom row), however, exhibit confinement dependences on $I_p$ and $B_T$ that are dissimilar from those of the HeGDC+B plasmas, but which are similar to those in conventional aspect ratio tokamaks, as embodied in the ITER98y,2 scaling,[6] with a strong $I_p$ dependence and a weak $B_T$ dependence.[18]

The dependence of thermal energy confinement and collisionality on the amount of lithium deposition in the Li scan is quite strong, as can be seen in Figs. 3a and b. The thermal energy confinement times are computed by the TRANSP[19,20] code. As is seen in Fig. 3a, the total thermal energy confinement, $\tau_{E,th}$, increases from 25 to 90 $ms$, and the electron energy confinement time, $\tau_{E,e}$, increases even more strongly, from 20 to over 100 $ms$, over the range of lithium deposition. The electron and ion collisionality, taken at $x = [\Phi/\Phi_a]^{1/2} = 0.7$ where $\Phi$, $\Phi_a$ are toroidal flux locally and at the plasma edge respectively, shows a strong reduction with increasing lithium deposition, as is seen in Fig. 3b. When the trends in Figs. 3a and b are combined, a strong inverse dependence of confinement time on collisionality emerges. This is seen in Fig. 3c where the normalized confinement time $B_T \tau_{E,th}$ is seen to scale with collisionality as $\nu_e^{*\ -0.67\pm0.14}$. For the confinement time scalings, the collisionality value at x=0.5 is chosen as representative of the average collisionality across the profile. The

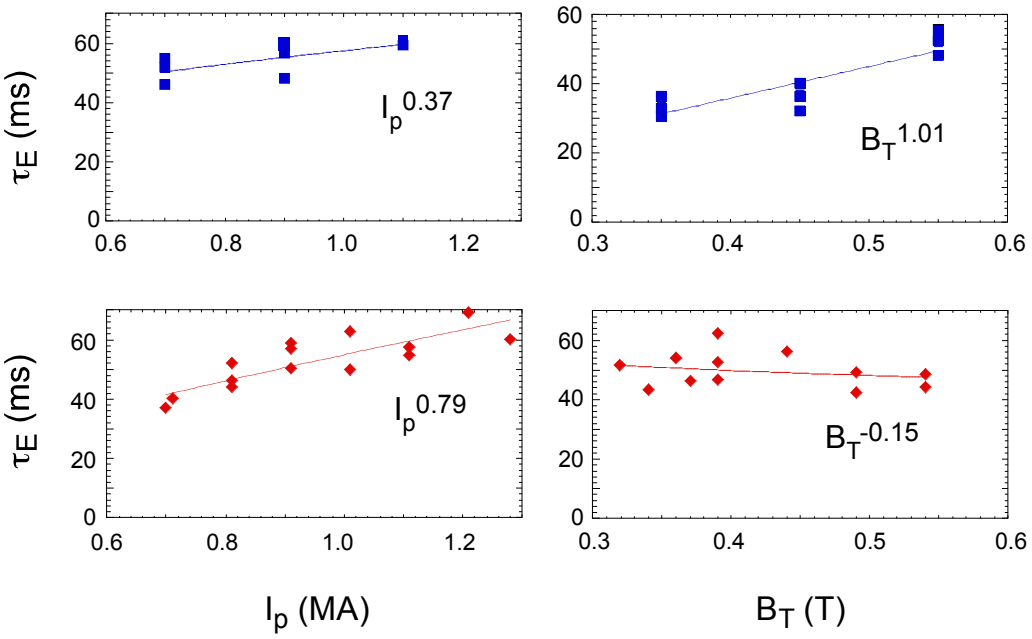


Figure 2: Thermal energy confinement scaling dependences of HeGDC+B discharges (top row) and Li EVAP discharges (bottom row) on plasma current and toroidal magnetic field.

general trend shown in Fig. 3c remains even if collisionality at a different radius is used. To put the variation shown in Fig. 3c into perspective, the variation of $B_T\tau_{E,th}$ from the ITER98y,2 scaling with collisionality is very weak, going as $\nu_e^{*\ -0.01}$.[5]

Isolating the relation between $B_T\tau_{E,th}$ and collisionality in a simple manner is dependent on having other physics parameters, such as $q$, $\langle\beta_T\rangle$, etc. held fixed. While most of these parameters, as well as engineering parameters, are held fixed in the Li scan, not all were. Plotted in Fig. 4a is the variation of the gyroradius $\rho_s(\propto T_e^{1/2}/B_T)$ and $c_s(\propto T_e^{1/2})$ across the range of collisionality at x=0.7 for the Li scan discharges. Here, $\rho_s$, a dimensional quantity, and $\rho^*$, a dimensionless quantity, are used interchangeably since the minor radius $a$ was the

same for all discharges in the scan. As can be seen in Fig. 4a, both $\rho_s$ and $c_s$ increase by approximately a factor of two going from high to low collisionality. The change in these parameters is due primarily to a broadening of the $T_e$ profile going from high to low $\nu_e^*$, as can be seen in Fig. 4b. The $T_e$ profiles are color-coded by the value of collisionality at x=0.7. Overall, the greatest increase in $T_e$ occurs in the x=0.5 to 0.8 spatial range.

Although the variation in $\rho_s$ is expected to influence the confinement time scaling, it can be taken into account using the dimensionless scaling, $\Omega\tau_E = \rho^{*(-\alpha)} f(\nu,\ \beta,\ q,\ \kappa, ...)$ where $\Omega$ is gyrofrequency ($\propto B_T$) and $\alpha$=2 for Bohm-scaling and $\alpha$=3 for gyroBohm scaling. The scaling in Fig. 3c can be recalculated using $\rho^{*\alpha}\Omega\tau_E$ as the independent parameter, and this is shown in Figs. 5a and b for $\alpha$=2 and 3 respectively. It is seen that because $\rho^*$ increases strongly with decreasing collisionality, the dependence on $\nu_e^*$ of the normalized confinement time with the additional Bohm or gyroBohm normalization is much stronger than for $B_T\tau_{E,th}$ without the $\rho^*$ correction for both scans. This is especially true using the gyroBohm assumption, with the normalized confinement scaling with collisionality as ${\nu_e^*}^{-1.50\pm0.18}$ and ${\nu_e^*}^{-1.91\pm0.22}$ for the Bohm ($\alpha$=2) and gyroBohm ($\alpha$=3) assumptions respectively. Previous analysis of HeGDC+B discharges indicated this dataset to be more consistent with the gyroBohm than the Bohm assumption.[1]

For discharges in the Nu scan, which is composed of both HeGDC+B and Li EVAP plasmas, physics variables such as $q$, $\langle\beta_T\rangle$ and $\Omega$, in addition to $\rho^*$, varied considerably due to the variations in both $B_T$ and $I_p$ in this collection. The $\Omega$ variation is taken into account by using the normalized confinement time, $\Omega\tau_{E,th}$ ($\propto B\tau_{E,th}$). The $q$ and $\langle\beta_T\rangle$ variations were minimized by choosing a set of discharges within as small a $q$ and $\langle\beta_T\rangle$ range as possible, but still having a reasonable number of points to describe the scaling of normalized confinement time with collisionality. This has been done by constraining the data to a $q_{r/a=0.5}$ range of 2 to 2.5 and a $\langle\beta_T\rangle$ range of between 8.5 and 12.5%. $\kappa$ was already constrained to 2.2 to 2.4 for these discharges. Normalized confinement times for the Nu scan as a function of collisionality are shown Figs. 6a-c for $\alpha$=0, 2 and 3 respectively. In Fig. 6a-c, those discharges that used Li EVAP wall conditioning are in red, and those that used HeGDC+B conditioning are in blue. It is seen in the plots that the Li EVAP discharges generally have lower collisionality than those that used HeGDC+B, extending that range of collisionality to lower values by almost an order of unity. The collisionality is seen to unify the confinement trends of these discharges, despite the different dependences on engineering variables, with a smooth and strongly favorable trend of increasing normalized confinement with decreasing collisionality. In Fig. 6a, it is seen that $B_T\tau_{E,th} \sim {\nu_e^*}^{-0.79\pm0.10}$. The scalings as a function

of $\nu_e^*$ are even stronger when the variation of $\rho^*$ is taken into account through the Bohm (Fig. 6b) and gyroBohm (Fig. 6c) assumptions, with the normalized confinement going as $B_T\tau_{E,th} \sim \nu_e^{*\ -1.06\pm0.12}$ and $B_T\tau_{E,th} \sim \nu_e^{*\ -1.21\pm0.16}$ respectively.

The variation of $n_e$, $Z_{eff}$, and $T_e$ in both the Nu and the Li scans was studied to determine which parameter(s) are primarily responsible for variation in $\nu_e^*$. This study was done for local parameters at x=0.7. For these local studies, a slightly different set of Nu scan discharges were chosen in order to ensure small ranges of both q and $\langle\beta_T\rangle$ at that location. x=0.7 was chosen since the results and analyses to be presented focus on the "confinement" region of the plasma. As was seen in Fig. 4b, it is within this region where the $T_e$ profile exhibited the greatest change with $\nu_e^*$. It was found that neither the density nor $Z_{eff}$ varied in such a magnitude or fashion to explain the variation in $\nu_e^*$. As can be seen in Fig. 7a and b, both $n_e$ and $Z_{eff}$ vary very little over the range of collisionality for both the Nu and Li scans. A linearly proportional relationship would be expected if either of these variables were controlling factors, since $\nu_e^* \propto n_e Z_{eff}$.

The factor that influenced the collisionality the most was an increase in local electron temperature resulting from a $T_e$ profile broadening as $\nu_e^*$ decreased. This was seen in Fig. 4b and also seen in Figs. 8a and b. The $\nu_e^*$ decrease from ~0.8 to 0.1 at x=0.7 was driven by an increase in $T_e$ at x=0.7 from 250 to 650 $eV$ ($\nu_e^* \propto 1/T_e^2$). The temperature profile peaking factor, defined as $T_e(0)/\langle T_e\rangle$ (ratio of central to volume-averaged $T_e$) decreased from ~2.3 to 1.4 for both the Nu and Li scans.

## III. Local Transport

In this section, the dependences of electron and ion local transport will be discussed, with the ultimate aim of identifying mechanisms believed to be responsible for the transport throughout the range of collisionality being studied. We will focus on the outer region of the plasma ($x \geq 0.6$) since this is the region where changes with changing collisionality are most pronounced. As we saw in Figs. 8a and b, the electron temperature increased at x=0.7 with decreasing collisionality for both the Nu and Li scans. Indeed, for both scans, a broadening of $T_e$ across the profile, but primarily between x=0.5 and 0.8 was observed (Fig. Fig. 4b). This electron temperature profile broadening reflects a progressive reduction in the electron thermal diffusivity in the outer region of the plasma as collisionality decreased. The decrease of the electron thermal diffusivity in the Nu scan can be seen clearly in Fig. 9. The curves are

color-coded to be proportional to the collisionality for that discharge within the collisionality range studied. As can be seen in the figure, the electron thermal diffusivities decrease by approximately an order of magnitude over the range of collisionality at x=0.7, going from 10 $m^2/s$ at the highest collisionality to 1 $m^2/s$ at the lowest. The electron thermal diffusivities exhibit the same type of behavior for the Li scan, but in this scan the difference was even more dramatic, with $\chi_e$ decreasing from 20 $m^2/s$ to 0.7 $m^2/s$ at this location going from the highest to lowest collisionality.

The change in electron thermal diffusivity with collisionality can also be examined in a relative sense by normalizing $\chi_e$ to $\chi_{e,gyroBohm}=\rho_s^2 c_s/a$. This normalization takes into account changes in $\rho_s$ and ion sound speed $c_s$ due to changes in $T_e$ to reflect the transport levels relative to what may be expected by gyroBohm transport. The profiles of $\chi_e/\chi_e$,gyroBohm are shown in Fig. 9b in arbitrary units, and similar to the trend observed for $\chi_e$ alone, the normalized transport decreases over an order of magnitude, due to the additional increase of $\chi_{e,gyroBohm}$ with decreasing $\nu_e^*$. A similar result is found for the Li scan as well.

Ion transport behaves differently from that of electrons. Fig. 10a shows the ion thermal diffusivity normalized by the neoclassical ion thermal diffusivity as computed by NCLASS[21] for both scans at x=0.60. This particular radius was chosen for this comparison to avoid regions of sharp gradients in the ion temperature that existed farther out in some of the discharges. While there is clearly scatter in the data, $\chi_i/\chi_{i,neo}$ increases approximately a factor of five to ten going from high to low collisionality, a trend that is reversed from that of the electron transport. At the highest collisionality, $\chi_i/\chi_{i,neo} \sim 0.5$, which we take to be at a neoclassical level when the differences among neoclassical theories and the uncertainty in $\chi_i$ ($\geq$ factor of 2) are taken into account. As collisionality decreases, the ions become more anomalous, with $\chi_i/\chi_{i,neo}$ reaching a factor of four to five.

The ion transport is also strongly dependent on the toroidal rotation and the rotation shear. The local toroidal flow velocity increases but the toroidal flow shear decreases as collisionality decreases. This is due to a relative broadening in the toroidal flow velocity profiles at this location as collisionality decreases. Fig. 10b shows the relation between the normalized ion transport and the flow shear, as characterized by the normalized gradient of the toroidal Mach number $M_s$. Here $\nabla M_s = R^2 \nabla\omega/c_s$, where $\omega$ is the local toroidal angular velocity. As can be seen, as the flow shear tends toward zero, the normalized ion transport increases; this occurs at low collisionality. This trend may reflect the role of flow shear ($E_r \times B$ shear) in suppressing low-k turbulence that can drive anomalous ion transport in NSTX, as observed in earlier analysis of another set of discharges.[22]

## IV. Linear Gyrokinetic Results

It has been shown previously that both low-k microtearing modes and high-k ETG modes are candidates for driving the anomalous electron energy transport outside the very core region of NSTX plasmas.[23–25] In particular, microtearing has dominated in high-$\beta$ plasmas,[23] while ETG modes tend to be more important at low-$\beta$.[24,25] While the discharges used in these studies qualify as high-$\beta$, the strength of both microtearing and ETG modes as a function of collisionality will be investigated. Starting first with the short wavelength ETG modes, one simple way of assessing their importance is to compare the measured electron temperature gradient to the critical gradient for ETG destabilization.[26] While this critical gradient formulation was developed for high aspect ratio, it was shown to be a good indicator for ETG destabilization even in the low aspect ratio NSTX.[24] The $T_e$ profile gradients, as characterized by $R/L_{Te}$, normalized to the critical gradient (also in terms of $R/L_{Te}$) exhibits approximately a factor of five reduction with decreasing collisionality near x=0.7 in the Li scan, decreasing from near 10 to near 1. Farther in, the ratio <1 (indicating stability to ETG modes) and farther out the ratio remains near 1. This is seen in Fig. 11 For the Nu scan, the ratio actually increases with decreasing collisionality near x=0.7; however, the ratio is <1, indicating stability to ETG modes. Farther in, the ratio decreases by approximately one order of magnitude to values <1. Linear gyrokinetic calculations by GYRO,[27] indicate that for both the Nu and Li scans, the ETG growth rates decrease with decreasing collisionality, with the ETG becoming completely stable for lower $\nu_e^*$.[28] It is important to note, however, that it is not the lower collisionality itself that stabilizes the ETG[29]; it is the reduction of $R/L_{Te}$ with decreasing $\nu_e^*$ that leads to the ETG stabilization.

The results of linear GYRO gyrokinetic calculations for low wavenumbers in representative low and high collisionality discharges from the Nu scan is shown in Figs. 12a and b. The high collisionality discharge (left panel) used HeGDC+B wall conditioning while the low collisionality discharge (right panel) used Li evaporation.The results for x=0.6 and 0.7 are shown. Previous analysis results for HeGDC+B discharges alone have shown that microtearing modes were an important component of the electron transport at these wavenumbers, and the decrease in electron transport going from high to low collisionality was associated with the stabilization of the microtearing modes.[23,28] The results in both the Nu and Li scans support this conclusion, and broadens it by considering the variation to the lower collisionality achieved in the Li EVAP discharges. Fig. 12a and b shows that the microtearing modes (solid lines) are strong and dominant, and much greater than the normalized $E_r \times B$ shearing rate at the high collisionality. They are suppressed, however, at low $\nu_e^*$, as evidenced

by a strong reduction in growth rate, especially at x=0.6. The residual microtearing that exists at low $\nu_e^*$ exhibits a narrower $k_\theta \rho_s$ space over which it is unstable, and the growth rates are comparable to the $E_r \times B$ shearing rates. On the other hand, an unstable region of a mode identified as a hybrid Trapped Electron Mode/Kinetic Ballooning Mode - TEM/KBM - (dashed curves), actually expands in radius going from high to low collisionality, although both at x=0.6 and 0.7, the normalized growth rates are comparable to the normalized $E_r \times B$ shearing rates. The change in the growth rate of this hybrid mode is not due to a large change in $Z_{eff}$ with collisionality; $Z_{eff} \simeq 2.75$ for the high $\nu_e^*$ discharge while $Z_{eff} \simeq 3.05$ at low collisionality. The hybrid mode in this region of the plasma us believed to drive ion and some electron transport, and is discussed more in a related paper.[29] The increased importance of these ion scale modes is consistent with the increase in anomalous ion transport going from high to low collisionality.

This general result is seen also for the Li scan (Fig. 13a and b), although with some more subtlety. The microtearing mode at x=0.6 (solid black line) is seen to persist both at high and low collisionality. In fact, its normalized growth rate is much lower relative to the normalized $E_r \times B$ shearing rate in the high than in the low collisionality case (where the two are nearly comparable). So, the microtearing may still play somewhat of a role in the electron transport in this scan; non-linear calculations are underway to assess the level of transport induced by these modes. The hybrid TEM/KBM, similar to that seen to exist in the Nu scan (Fig. 13), exhibits increased growth and an expanded region of instability going from the high to the low collisionality case, again consistent with the increase in the level of anomalous ion transport in this scan as well. Here too, non-linear calculations are underway to assess the level of transport induced by these modes.

## V. Summary

Although plasmas using different wall conditioning techniques exhibit different confinement scalings with engineering parameters, collisionality has been found to unify the confinement trends. The data presented in this work come from discharges using HeGDC+B wall conditioning as well as lithium evaporation for wall conditioning, the latter technique extending the achievable collisionality range to lower values by almost an order of unity. The normalized confinement times are found to exhibit a strong and favorable scaling with decreasing $\nu_e^*$ when holding most other global dimensionless variables (q, $\beta_T$) fixed or limiting their range as much as possible. Taking the variation of $\rho^*$ across the range of collisionality into account actually makes the confinement dependence even stronger when either Bohm or

gyroBohm transport is assumed. The reduction in transport with decreasing collisionality is due primarily to an improvement in the electron channel, as reflected by a broadening of the electron temperature profile going from high to low collisionality. Analysis indicates that ETG modes become completely suppressed for the lower collisionality discharges due to the $T_e$ broadening, and microtearing mode growth rates are reduced and exhibit a reduced extent of instability in both wavenumber and real space. The reduction in electron transport more than compensates for an increase in the anomalous ion transport, apparently due to the growth and expansion of a hybrid TEM/KBM mode in the outer region of the plasma at low collisionality. Rotation shear decreased as collisionality decreased, and non-linear analysis is underway to assess the impact of this on the level of ion transport. Extrapolating these results to even lower collisionalities representative of ST-based FNSFs is difficult, but will be addressed in experiments on NSTX-Upgrade. It will be important to understand whether the electron transport will continue to improve as collisionality is reduced further, as well as understanding the role of the hybrid TEM/KBM at lower $\nu_e^*$. Whether it is collisionality that controls how anomalous the ion transport is, or whether the ion transport level is tied more tightly to the $E_r \times B$ shear, will be explored in NSTX-U with its expected operation at lower collisionality and its multi-aiming NBI giving flexibility to control rotation and rotational shear.

**Acknowledgements** This work has been supported by U.S. Dept of Energy contracts DE-AC02-09CH11466 and DE-AC05-00OR22725.

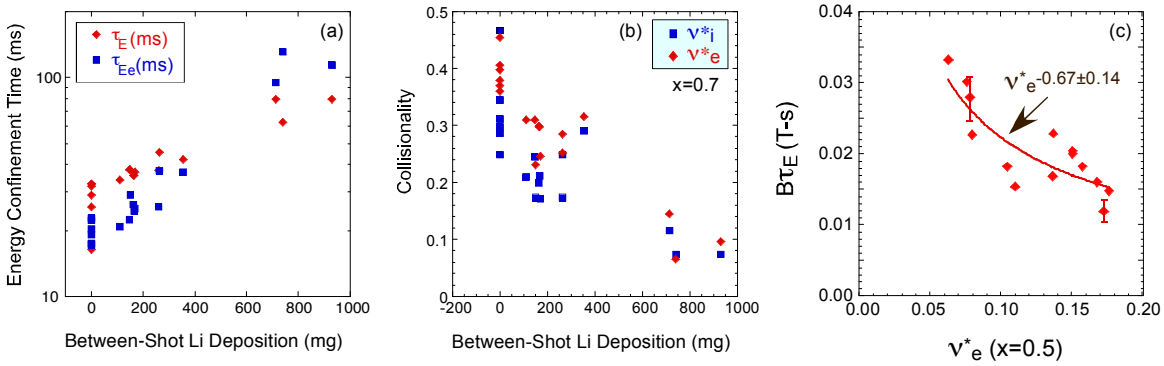


Figure 3: a) Total thermal and electron energy confinement , and b) ion and electron collisionality at x=0.7 as functions of the between-shot lithium deposition for the Li scan data. c) Normalized confinement time, $B_T \tau_{E,th}$ , versus electron collisionality at x=0.5 for the Li scan data.

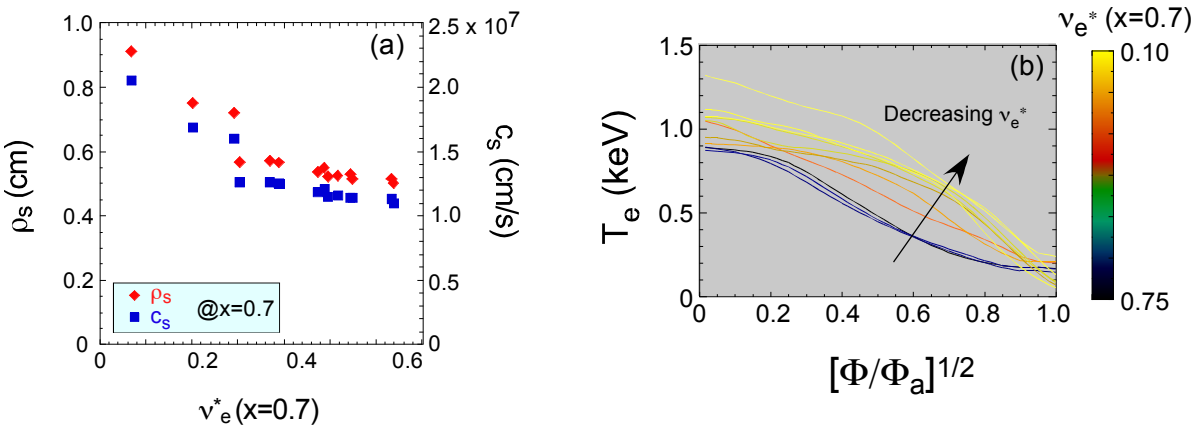


Figure 4: a) $\rho_s$ (blue points) and $c_s$ (red points) as a function of $\nu_e^*$ at x=0.7 for the Li scan. b) $T_e$ profiles for the Li scan color-coded by $\nu_e^*$ at x=0.7.

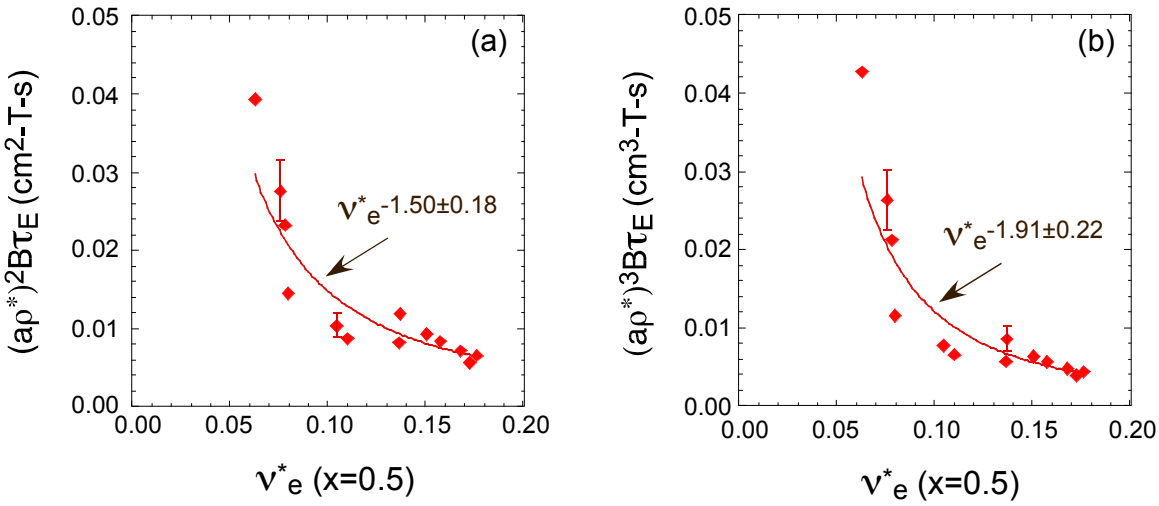


Figure 5: Normalized confinement time as a function of collisionality at x=0.5 for the Li scan for a) Bohm and b) gyroBohm $\rho_s$ dependences.

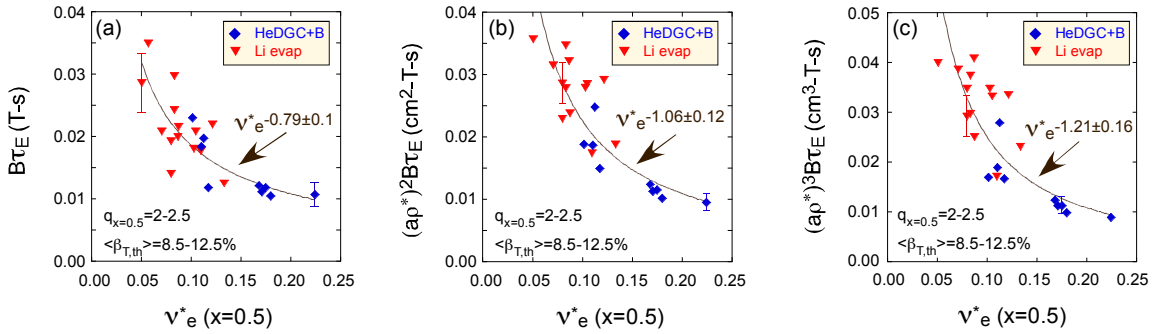


Figure 6: Normalized confinement time as a function of collisionality at x=0.5 for the Nu scan for $\alpha$= a) 0, b) 2 and c) 3. Blue points are from discharges that used HeGDC+B wall conditioning, while red points are from discharges that used Li EVAP.

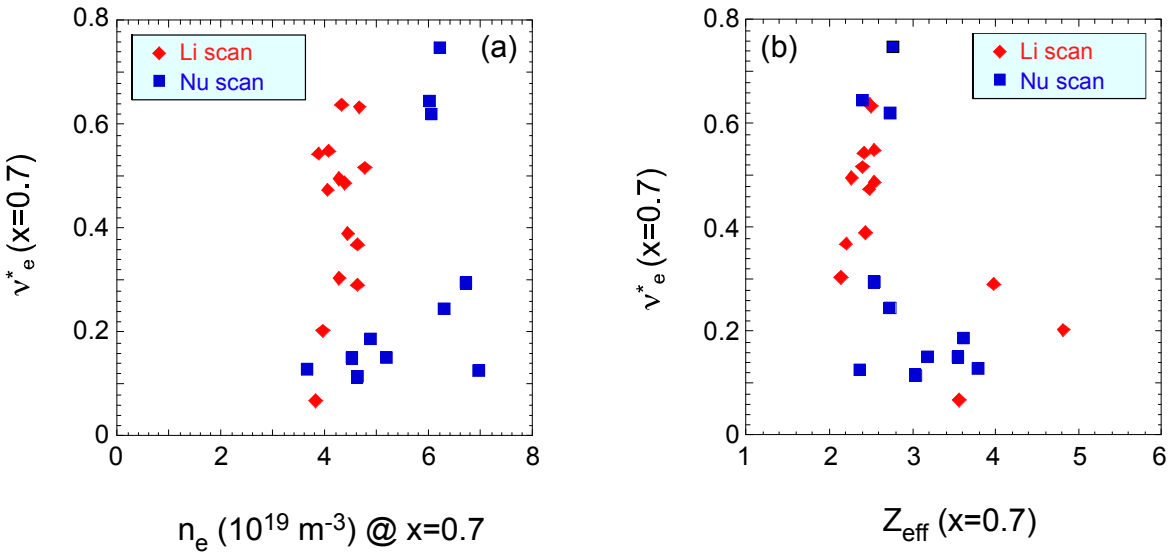


Figure 7: Variation of collisionality with a) $n_e$ and b) $Z_{eff}$ for the Nu (blue points) and Li (red points) scans. All values are taken at x=0.7.

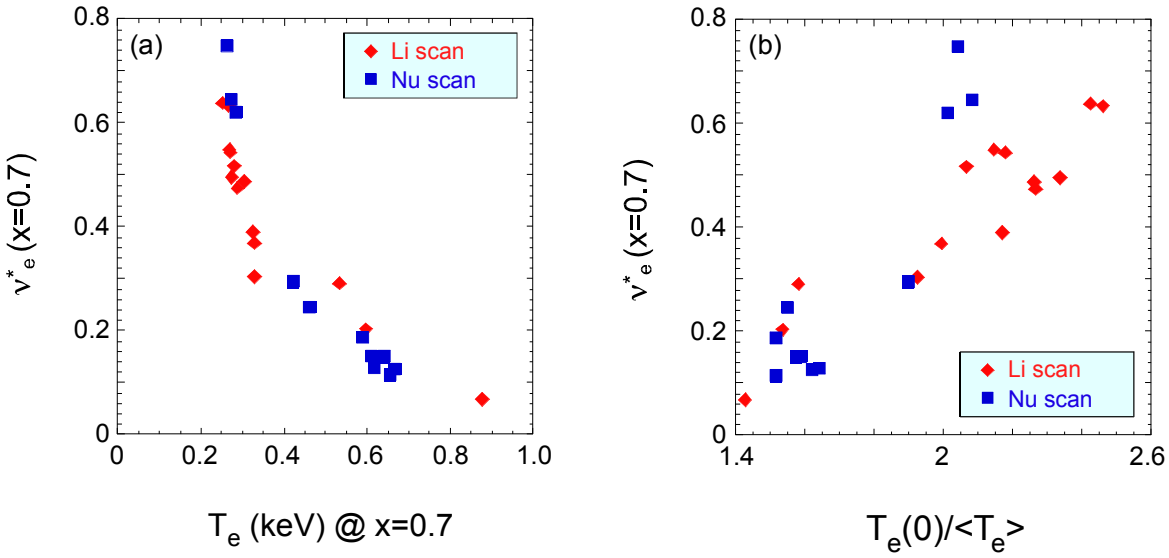


Figure 8: Variation of collisionality with a) $T_e$ at x=0.7 and b) electron temperature profile broadness, $T_e(0)/ < T_e >$ for the Nu (blue points) and Li (red points) scans.

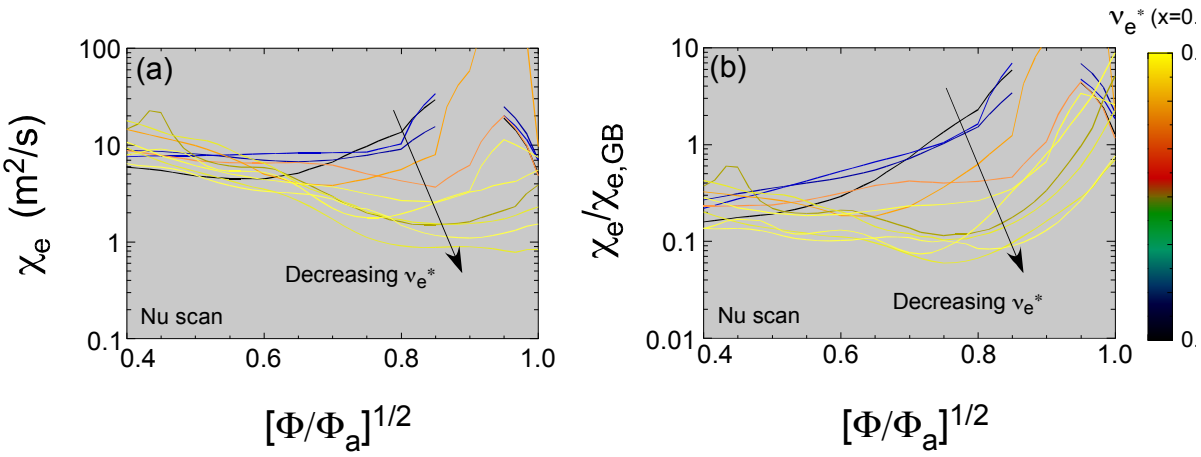


Figure 9: a) $\chi_e$ profiles color coded by electron collisionality at x=0.7 for the Nu scan. b) $\chi_e$ profiles normalized to the local $\chi_{e,gyroBohm}$ ($\propto \rho_s^2 c_s/a$), color coded by electron collisionality at x=0.7.

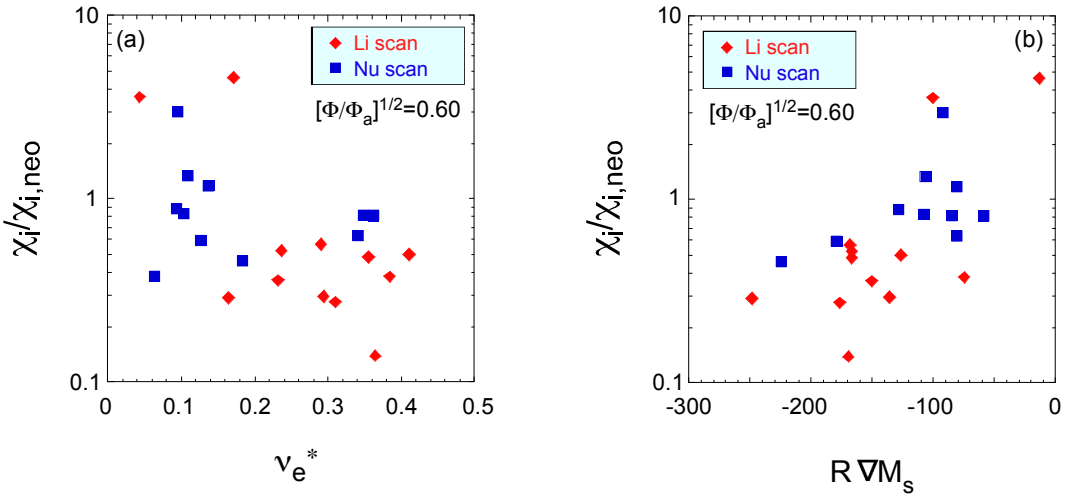


Figure 10: a) Ion thermal diffusivity, $\chi_i$ normalized to the neoclassical ion thermal diffusivity as determined by NCLASS as a function of $\nu_e^*$ at x=0.6. b) $\chi_i/\chi_{i,neo}$ as a function of $\nabla M_s$ ($R^2\nabla\omega/c_s$ at x=0.6. Values from both the Nu scan (blue) and Li scans (red) are shown.

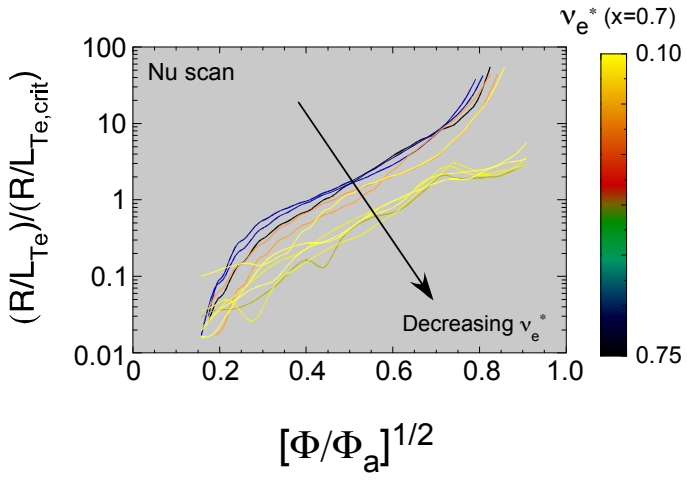


Figure 11: Experimental profiles of $R/L_{Te}$ normalized by the critical $R/L_{Te}$ for ETG stability[26] for the Nu scan. The curves are color-coded by the value of $\nu_e^*$ at x=0.7.

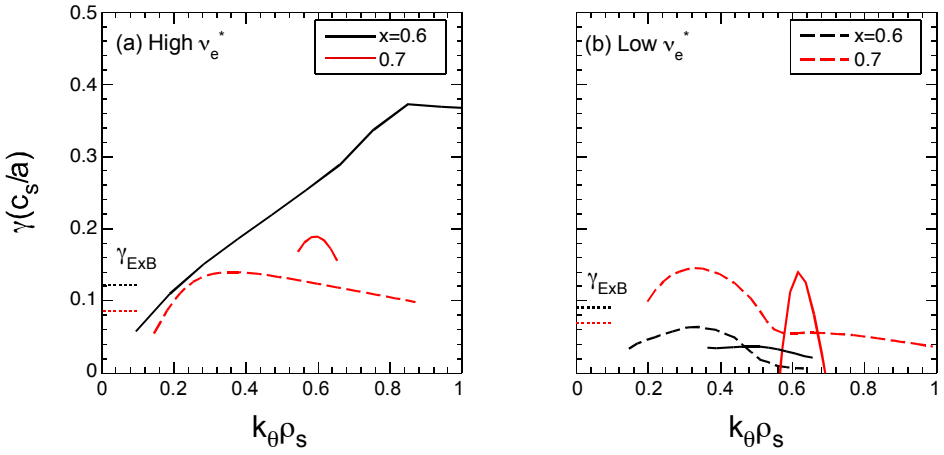


Figure 12: Normalized growth rates of low-k modes from linear GYRO runs for a) high and b) low collisionality cases in the Nu scan. The solid lines represent microtearing modes, while the dashed lines represent the hybrid TEM/KBM mode. The normalized $E_r \times B$ shearing rates for each radius are given by the color-coded horizontal dashed lines. Black lines for the growth and shearing rates are for x=0.6 and red are for x=0.7.

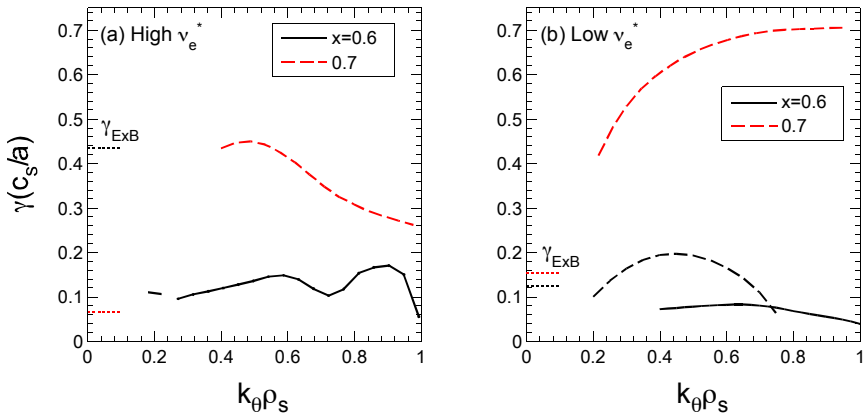


Figure 13: Normalized growth rates of low-k modes from linear GYRO runs for a) high and b) low collisionality cases in the Li scan. The solid lines represent microtearing modes, while the dashed lines represent the hybrid TEM/KBM mode. The normalized $E_r \times B$ shearing rates for each radius are given by the color-coded horizontal dashed lines. Black lines for the growth and shearing rates are for x=0.6 and red are for x=0.7.

## References


[1]KAYE, S.M., M.G. Bell, R.E. Bell, et al., Nucl. Fusion **46**, 848 (2006).

[2]KAYE, S.M., R.E.. Bell, D. Gates, et al., Phys. Rev. Lett. **98**, 175002 (2007).

[3]KAYE, S.M., F.M. Levinton, D. Stutman, et al., Nucl. Fusion **47**, 499 (2007).

[4]CONNOR, J.W., Plasma Phys. Controlled Fusion **30**, 619 (1988).

[5]PETTY, C.C., Phys. Plasmas **15**, 080501 (2008).

[6]ITER Physics Basis, Nucl. Fusion **39**, 2137 (1999).

[7]KUGEL, H.W., D. Mansfield, R. Maingi, et al., Journ. Nucl. Materials **390**, 1000 (2009).

[8]PODESTA, M., R.E. Bell, A. Diallo et al., Measurements of core lithium concentration in diverted h-mode plasmas of NSTX, submitted to Nuclear Fusion, 2012.

[9]BELL, M.G., H.W. Kugel, R. Kaita, et al., Plasma Phys. Controlled Fusion **51**, 124054 (2009).

[10]DING, S., S.M. Kaye, R.E. Bell, et al., Plasma Phys. Controlled Fusion **52**, 015001 (2010).

[11]MENARD, J.E., L. Bromberg, T. Brown, et al., Nucl. Fusion **51**, 103014 (2011).

[12]PENG, Y.K.M., J.M. Canik, S.E. Diem, et al., Fusion Science and Technology **60**, 441 (2011).

[13]MAINGI, R., S.M. Kaye, C.H. Skinner, et al., Phys. Rev. Lett. **107**, 145004 (2011).

[14]MAINGI, R., D.P. Boyle, J.M. Canik, et al., Nucl. Fusion **52**, 083001 (2012).

[15]MAINGI, R., T.H. Osborne, B.P.LeBlanc, et al., Phys. Rev. Lett. **103**, 075001 (2009).

[16]VALOVIC, M., R. Akers, G. Cunningham, et al., Nucl. Fusion **49**, 075016 (2009).

[17]VALOVIC, M., R. Akers, M. deBock, et al., Nucl. Fusion **51**, 073045 (2011).

[18]GERHARDT, S.P., D.A. Gates, S.M. Kaye, et al., Nucl. Fusion **51**, 073031 (2011).

[19]HAWRYLUK, R. J., An empirical approach to tokamak transport, in Physics of Plasmas Close to Thermonuclear Conditions: Proceedings Course (Varenna 1979) vol. 1, page 19, 1980.

[20]PANKIN, A., D. McCune, R. Andre et al., Computer Physics Communications **159**, 157 (2004).

[21]HOULBERG, W.A., K.C. Shaing, S.P. Hirshman, et al., **4**, 3230 (1997).

[22]KAYE, S.M., W. Solomon, R.E. Bell, et al., Nucl. Fusion **49**, 045010 (2009).

[23]GUTTENFELDER, W., J. Candy, S.M. Kaye, et al., Phys. Rev. Lett. **106**, 155004 (2011).

[24]MAZZUCATO, E., D.R. Smith, R.E. Bell, et al., Phys. Rev. Lett. **101**, 075001 (2008).

[25]REN, Y., S.M. Kaye, E. Mazzucato, et al., Phys. Rev. Lett. **106**, 165005 (2011).

[26]JENKO, F., W. Dorland, G.W. Hammett, et al., **8**, 4096 (2001).

[27]CANDY, J., E. Belli, General Atomics Technical Report No. GA-A26818, 2012.

[28]GUTTENFELDER, W., J. Candy, S.M. Kaye, et al., **19**, 056119 (2012).

[29]GUTTENFELDER, W., J. Candy, S.M. Kaye, et al., Progress in simulating turbulent electron thermal transport in NSTX, submitted to Nuclear Fusion, 2012.

The Princeton Plasma Physics Laboratory is operated
by Princeton University under contract
with the U.S. Department of Energy.

Information Services
Princeton Plasma Physics Laboratory
P.O. Box 451
Princeton, NJ 08543

Phone: 609-243-2245
Fax: 609-243-2751
e-mail: pppl_info@pppl.gov
Internet Address: http://www.pppl.gov